ORIGINAL PAPER

A reduced-order model based on the coupled 1D-3D finite element simulations for an efficient analysis of hemodynamics problems

**Eduardo Soudah · Riccardo Rossi · Sergio Idelsohn ·
Eugenio Oñate**

Abstract   A reduced-order model for an efficient analysis of cardiovascular hemodynamics problems using multiscale approach is presented in this work. Starting from a patient-specific computational mesh obtained by medical imaging techniques, an analysis methodology based on a two-step automatic procedure is proposed. First a coupled 1D-3D Finite Element Simulation is performed and the results are used to adjust a reduced-order model of the 3D patient-specific area of interest. Then, this reduced-order model is coupled with the 1D model. In this way, three-dimensional effects are accounted for in the 1D model in a cost effective manner, allowing fast computation under different scenarios. The methodology proposed is validated using a patient-specific aortic coarctation model under rest and non-rest conditions.

Keywords   Blood flow · Boundary conditions ·
Reduced-order models and Aortic coarctation

1 Introduction

The simulation of blood flow problems assumes a large importance in biomechanics due to the many potential fields of application. The use of realistic boundary conditions is essential to guarantee the performance and the accuracy of numerical simulations, especially in cardiovascular prob-

E. Soudah · R. Rossi · S. Idelsohn · E. Oñate
International Center for Numerical Methods in Engineering (CIMNE),
Technical University of Catalonia, 08034 Barcelona, Spain
e-mail: esoudah@cimne.upc.edu

S. Idelsohn (✉)
Institució Catalana de Recerca i Estudis Avançats (ICREA),
Barcelona, Spain
e-mail: sergio@cimne.upc.edu

lems. In particular, the flow in arteries depends strongly on the outflow boundary conditions which model the downstream domain. The application of constant tractions as outlet boundary conditions for 3D domains represents the simplest possibility. Unfortunately, such conditions are not realistic and cause spurious pressure waves to become in the solution. Such waves travel along the artery network and distort the numerical solution. An efficient technique is thus needed to minimize these effects. Sophisticated outlet boundary conditions [29,30] aimed to minimizing such problem can be found in the literature. Others authors address the problem by applying geometrical multiscale modeling [4,7,9,17,34,36]. These approaches typically consist in the combination of models with different levels of approximation (3D, 1D and 0D models) each aimed at capturing particular features of the solution. 3D models are applied in regions where details of the local flow are needed. This is typically the case when the flow is strongly three dimensional or it tends to be turbulent. 1D models are typically used in the up-downstream domain of the 3D models, so that the whole arterial network can be described efficiently taking into account flow propagation effects. Zero dimensional models (or lumped models) are generally used to describe the lower level of the cardiovascular system or to model the heart. A typical problem that rises at the interface between the 1D and 3D domains is the mapping of the parabolic velocity distribution (assumed in the 1D model) to an "equivalent" distribution on the 3D inlet. Such mapping is not trivial since the discretized 3D model is generally not exactly circular. A proposal to solve the impasse can be found in [2]. In current work we opted for the simpler (but less accurate) option of applying a spatially uniform inlet velocity, with a total flow corresponding to the one of the 1D. This is only acceptable since our aim is not to compute the Wall Shear Stress (WSS) but rather to estimate the dissipation induced by the non-standard topol-

ogy of the artery or area of interest. We also observe that the method we propose works under the assumption that the 3D inlet and outlet boundaries are approximately perpendicular to the centerline of the artery and positioned at points in which the flow can be reasonably approximated as 1D. It is interesting to remark that, as observed in the extensive review paper [18,31], the reliable computation of WSS, which is often the target of CFD simulations, depends on the availability of a sufficiently fine discretization of the boundary layer and is sensibly affected by the Fluid-Structure Interaction of the flow with the artery boundaries. The idea we leverage in the current work is that the extra dissipation induced by severe variations of the geometry is dominated by the appearance of turbulent effects within the volume. The evaluation of such effect requires a sufficiently fine discretization of the volume but does not put the extra requirements on the boundary layer mesh, and shall not be severely affected by the deformability of the walls, hence allowing the assumptions of considering the walls rigid which greatly simplifies the simulation and reduces the runtime. In [25] an extensive review of the most popular 1D models can be found. Recently, new models have been proposed [1,20,22,28] improving the viscoelastic behavior of the walls. However, the 1D models alone are not capable to capture in an effective way the energy losses due to the 3D geometrical shapes of the arteries, e.g, in stenotic arteries, aneurysms or other cardiovascular pathologies, such as aorta coarctation. Nevertheless, to discretize the whole 3D cardiovascular domain or coupled fluid-structure interaction (FSI) modeling is computational expensive and unfeasible in practical applications due to the numerical challenges involved. Despite its modeling shortcomings, geometrical multiscale models combined with patient-specific geometries remains the predominant approach for vascular blood flow. Such models allow quantifying the hemodynamics variables such as, flow reversal, flow separation and wall shear stress areas over the arterial wall in a non-invasive way useful for clinicians. Notable exceptions include the work of [29,32,33] on cerebral aneurysms.

In this paper, we propose a reduced-order Computational Fluid Dynamics (CFD) model specifically aimed to the estimation of the pressure gradient and the energy losses induced by stenosis in cardiovascular scenarios. The key features of our approach are: (1) a patient-specific anatomy and a computational mesh obtained during a routine clinical imaging session; (2) a coupled multiscale 0D-1D-3D model to approximate the energy losses induced by a narrowing of the artery lumen. The solution of the 3D model is used to train a reduced-order model which is aimed to capturing the pressure drop within two sections located upstream and downstream of the stenosis. Then the reduced-order model is integrated within the 1D model to create a 1D reduced-order model. Such model is able to simulate the energy losses and the flow distribution taking into account the patient-specific anatomy

in real time under different scenarios. The ultimate goal is to validate the CFD framework with the energy losses through an aortic coarctation (CoA) under resting and non-resting conditions of the patient. CoA of the aorta occurs approximately in 10 % of patients with congenital heart defects and represents a narrowing of the descending aorta. Due to the reduction in the aorta descending diameter, high pressure gradients can appear across the CoA, resulting in an increased cardiac workload in the left ventricle during systole [14]. Investigation into the hemodynamics and bio-mechanical basis of the morbidity in CoA shows that the pressure gradient is dependent on the aorta area reduction, the flow rate and the physiological state of the patient: during non-rest conditions the pressure gradient can increase considerably and can provoke heart failure [13]. To measure the pressure gradient under these non-rest conditions, that are difficult to replicate in a clinic environment, is a biomedical challenge [3]. For is reason, a procedure that combines patient-specific image data and numerical tools to further understand the hemodynamics alterations, under resting and non-resting situations will allow clinicians to improve the diagnosis and define which should be the CoA treatment for the patient [14,23]. Some authors have used CFD models to study the hemodynamics in the CoA [12,13]. However, different numerical approaches might lead to different pressure predictions. The reduced-order methodology described in this paper has been implemented as part of the C++ finite element library KRATOS (www.cimne.com/kratos) [5]. KRATOS is a multi-physics simulation open source (LGPL licence) framework based on the stabilized Finite Element Method for analysis of the Navier-Stokes equations in viscous flows. Efficient and parallel solvers for 3-D fluid-structure interaction (FSI) [6] problems have been implemented in KRATOS that allow tackling large problems using supercomputers if available.

2 Computational framework

As previously stated, realistic boundary conditions are essential for simulating a appropriately behavior of the blood flow propagation. In this section we define a 1D FSI model coupled to a reduced-order model for cardiovascular analysis. The methodology used consists on a two step process. The first step (training phase) consists in estimating correctly the pressure drop between two sections of a 3D model by solving a geometrical multiscale problem. From the numerical point of view, we embed a 3D domain into a 1D network in order to perform 3D simulations within a consistent hemodynamics conditions provided by a 1D FSI model. A lumped model is used to simulate the peripheral vascular beds of the cardiovascular system. Once the first simulation is completed, the pressure drop predicted by the 3D model is used to train the 1D reduced-order model via a least square fitting procedure.

Fig. 1 3D-1D coupled approach schematics. Γ_i are the interface surfaces
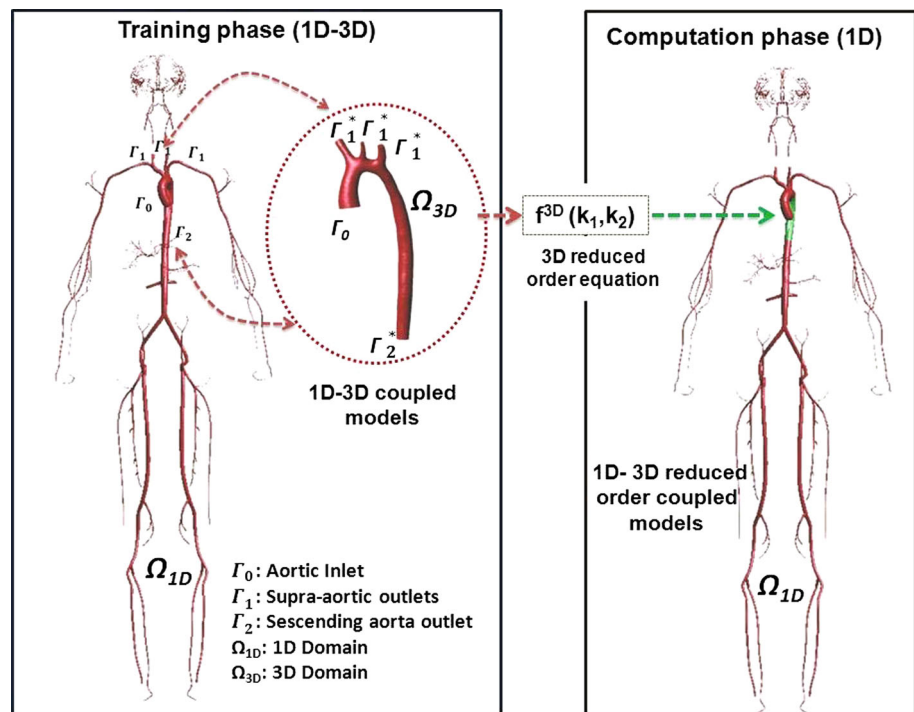
The trained model is thus able to estimate the energy losses between the two areas selected in the 3D model. Once the reduced-order model is defined, a coupled 1D FSI-reduced-order model will be capable of estimating the patient-specific pressure drop under different rest or non-rest situations. The second step (computing phase) consists in setting different boundary conditions for the coupled 1D FSI-reduced-order model to estimate the pressure drop (at any point) taking in account the 3D anatomical model. This will enable us to simulate different pathological situations taking into account the energy losses produced by the 3D model. Besides, this reduced-order approach brings down the computational costs significantly. The flow diagram of this scheme is shown in Fig. 1.

2.1 Mathematical model for the 1D reduced-order model

In this section we describe a non-linear 1D formulation and the reduced-order model proposed to account for the 3D effects caused by the patient-specific area of interest. In absence of branching, an artery may be considered as a cylindrical compliant tube which extends from z = 0 to z = L, where L is the the artery length. The artery takes into account the assumptions of axial symmetry, radial displacements, constant pressure on each section, no body forces and dominance of axial velocity. The governing system of equations for an incompressible newtonian fluid are derived by applying conservation of mass and momentum in a 1-D impermeable and deformable tubular control volume. These equations are:

$$\left(\frac{\partial \mathbf{A}}{\partial \mathbf{t}} + \frac{\partial \mathbf{Q}}{\partial \mathbf{z}} \right) = 0 \tag{1a}$$

$$\left(\frac{\partial \mathbf{Q}}{\partial \mathbf{t}} \right) + \frac{\partial}{\partial z} \left(\alpha \frac{Q^2}{A} \right) + \frac{\mathbf{A}}{\rho} \frac{\partial \mathbf{P}}{\partial z} + \mathbf{K_R} \left(\frac{Q}{A} \right) = 0 \tag{1b}$$

$$P_{ext} + \frac{Eh_o \sqrt{\Pi}}{1 - \mu^2} \frac{\sqrt{A} - \sqrt{A_o}}{A_o} = P \tag{1c}$$

where A(z,t) is the cross-sectional area of the vessel, Q(z,t) is the mean blood flow, P is the average internal pressure over the cross-section, α is the momentum-flux correction coefficient, z is the axial coordinate along the vessel, t is the time, ρ is the density of the blood taken as $1{,}050 \, \text{Kg/m}^3$ and K_R is the friction force per unit length, which is modeled as $K_R = 2\pi \cdot \nu(\gamma + 2)$ [8], with ν being the viscosity of the blood taken here as $4.5 \, \text{m} \cdot \text{Pa} \cdot \text{s}$. The vessel wall is modeled as a thin, homogeneous and elastic material. Parameters A_0 and h_0 in Eq. 1(c) are the sectional area and the wall thickness, respectively, at the reference state (P_0, U_0), with P_0 and U_0 assumed to be zero, E is the Young modulus and μ is the Poisson's ratio, typically taken as $\mu \approx 0.5$, which implies that the biological tissue is practically incompressible. In absence of detailed of patient-specific data, the wall elasticity and the thickness of the 55 largest arteries are based on data published by Wang and Parker [35]. At each domain decomposition, whether corresponding to a discontinuity in the mechanical or geometrical vessel properties, or to a cardiovascular branching, continuity of flow and of total pressure is enforced as follows:

$$Q_i = \sum_d (Q_j)_d \qquad (2)$$

$$P_i + \frac{1}{2}\rho\frac{Q_i^2}{A_i^2} = (P_j)_d + \frac{1}{2}\rho\frac{(Q_j^2)_d}{(A_j^2)_d} + (f^{3D}{}_j(k_1, k_2))_d \qquad (3)$$

where indexes i and j denote the parent and the daughter vessels respectively, and d indicates the number of system domains. Function $f^{3D}(k_1, k_2)$ denotes the energy losses of the 3D model, where k_1 and k_2 are obtained by fitting the pressure drop between the two planes defined in the 3D model. k_1 and k_2 are the viscous and turbulent coefficients that should be adjusted according to the pressure drop between the two planes defined in the 3D model. In this work we do not consider the inertial term. The system obtained is solved by a Newton iteration scheme, taking as the starting point the reference section area and flow, i.e:

$$f^{3D}{}_j(k_1, k_2) = k_1 Q_j + k_2 \mid Q_j \mid Q_j \qquad (4)$$

With simple manipulations of the differential Eq. (1) it is possible to obtain the conservative form for the temporal evolution of the flow and the vessels area and discretize the system obtained using a second order Taylor-Galerkin scheme. This scheme is appropriate for this problem as it can propagate waves of different frequencies without suffering from excessive dispersion and diffusion errors. A derivation of the 1D-FSI models can be found in [8] and [27]. The Taylor-Galerkin scheme requires a time step limitation in order to keep the solution stable. In this work the stabilization technique adopted has been the Courant Friedrichs Lewy condition (CFL condition) [21].

$$\Delta t \leq CFL \min_{0 \leq i \leq N} \left(\frac{h_i}{max(\lambda_{1,i}, \lambda_{1,i+1})} \right) \qquad (5)$$

where N is the number of the elements, h_i is the local element size and $\lambda_{1,i}$ indicates the value of the eigenvalue evaluated at the mesh i^{th} node of the matrix of the conservative form obtained from the derivation of the 1D-FSI model [8]. The CFL value adopted is 0.57 [21]. The 3D computational analysis is performed assuming that the arterial wall is rigid. Blood is considered as an homogeneous laminar Newtonian fluid modelled by the incompressible Navier-Stokes equations using the same density and dynamic viscosity as for the 1D model. Although these are important limitations, they make the simulation effort simpler. Furthermore, the knowledge of the patient-specific mechanical properties is quite difficult, consequently the objective of this work is to determine the pressure gradient in the anatomical domain using a reduced-order model based on multiscale modeling. Recent studies [15] use turbulence models to predict the kinetic energy due to the narrowing of the coarctation.

2.2 3D-1D Coupling interfaces

In order to keep the continuity in the area sections between the 3D and the 1D geometrical models, the diameters of the 1D geometrical model were firstly scaled taking into account a proportional diameter factor between the 3D and 1D geometrical models. The properties of the 1D geometrical models were taken from [35]. For the training phase, at each coupling 1D-3D interface we enforce the continuity of the flow and the total pressure (Eqs. 2, 3). This means that at every time step t_n we compute the velocity and the pressure using the 1D approach over the whole domain Ω_{1D}. Then, the variables over the interface sections (Γ_1, Γ_2) of the Ω_{1D}-Ω_{3D} domain are determined (Fig. 1). Following that, the 3D problem is solved in Ω_{3D} using the boundary conditions obtained in the Γ_1, Γ_2 sections from the 1D model. For the next time step ($t_n + 1$) the process is repeated until the final simulation time is reached. This coupling procedure is justified by the fact that the 1D domain can be considered as a passive element which absorbs the flow generated by the 3-D domain. During the training phase, pressure values at Γ_1 and Γ_2 interfaces are stored for each time step with the objective of estimating the coefficients k_1 and k_2 of Eq. 4 by the least squares method. We choose the value of $f^{3D}(k_1, k_2)$ that minimizes the sum of the squared pressure drop from the 1D flow values compared to the 3D values. In Sect. 3.1.3 we show a pressure drop of the 3D computational values versus the predictions of the reduced-order model (Fig. 3). For the computation phase, the coupled 1D coupled FSI—reduced-order model is solved by using the coefficients k_1 and k_2 estimated previously.

3 Study case: aorta coarctation

3.1 Training phase

3.1.1 Model anatomy, geometry and mesh

The physiological and geometrical data used in this work was obtained from [3].The patient was a 71 kg, 177 cm tall, 17-year old male with a mild thoracic aortic coarctation. Image data come from a 1.5-T Phillips scanner using a gadolinium-enhanced MR angiography (MRA) with the patient in the supine position. The 3D model (Fig. 2) includes the ascending aorta, aortic arch, descending aorta, left subclavii, brachiocephalic and finally left common carotid arteries in Stereo Lithography (STL) file format. To generate the 3D volume we used the pre and post-processor GiD [10]. GiD can be efficiently used for mesh generation in CFD analysis. For generating the 3D volume mesh from the STL file, we have used an isosurface stuffing procedure. This algorithm generates tetrahedral element form a small set of precomputed stencils. The boundary mesh is guaranteed to be a geo-

Fig. 2 Patient-specific anatomical model with a mild thoracic aortic coarctation (CoA). Ascending aortic flow waveforms (in cm^3/s) under rest conditions measured by the (PC)-MRI sequence and ascending aortic pressure (in mmHg) measured with a pressure catheter under rest conditions. The table shows the total flow (in L/min) and percentage of ascending aortic flow through the various branches of the aortic model under rest conditions

	Total Flow (L/min)	% AscAo
AscAo	3.71	100
BA	0.624	17
LCC	0.312	8
LC	0.364	10
DiaphAo	2.41	65
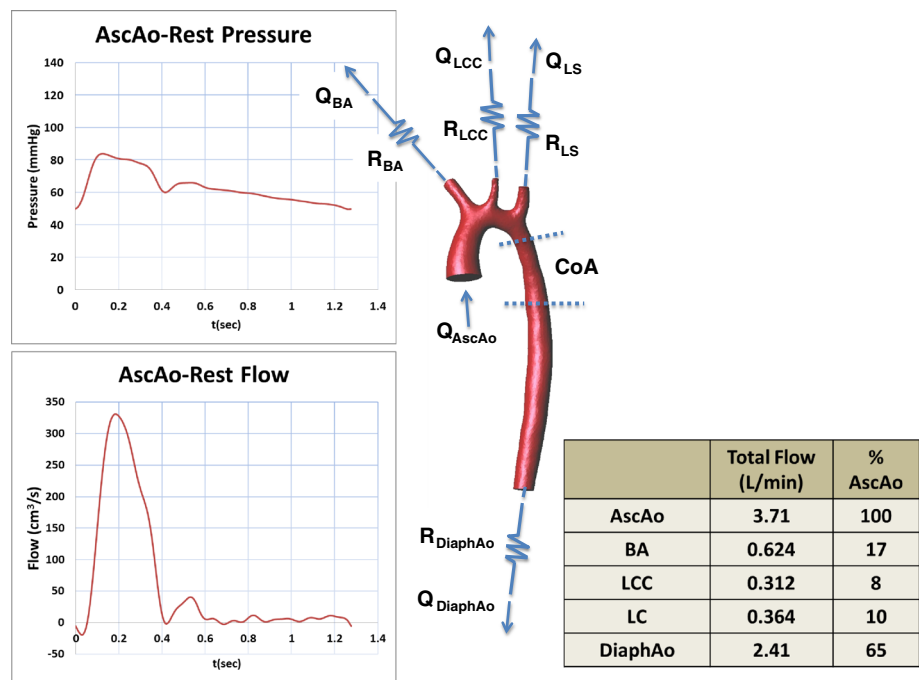
metrically and topologically accurate approximation of the isosurface [16]. This technique ensures tetrahedral volume elements with optimal angle and volume for the simulations. Using this method we have obtained smooth elements and an aspect radio for the whole mesh greater than 0.9 (the ideal ratio is one for an equilateral triangle). In this work we dont need a refined boundary layer mesh, due to the we have focused on the energy dissipation induced by the turbulence effects. In [18] other authors propose how to build a patient-specific models from medical images taking into account a fine discretization of the boundary layer in order to capture the WSS and OSI effects over the arterial wall. The result of the isostuffing procedure is a volume mesh of 4,322,556 four-noded tetrahedral elements and 206,880 three-noded triangles with 777,235 nodes. The original surface mesh has 138,532 linear triangles and 69,268 nodes. Figure 2 shows a rendering image of the 3D volume mesh. The 1D computational mesh contains 551 linear two-noded elements and 586 nodes.

3.1.2 Boundary conditions: inlet and outlet conditions at rest

Blood flow information [3] was acquired using a cardiac-gated, 2D, respiratory compensated, phase-contrast (PC) sequence with through-plane velocity encoding. The cardiac output of the patient was 3.71 L/min, the heart rate was 47 beats per minute (cardiac cycle T = 1.277 s). Figure 2 shows the blood flow and pressure waveforms at the ascending aorta (AscAo). The inlet velocity profile is prescribed as uniform and flat at the inlet surface. The quality of the waveforms

to the supra-aortic vessels (the Brachiocephalic artery (BA), the left common carotid artery (LCC) and the left subclavian artery (LS) arteries) was deemed too noisy to be used in the computations. Figure 2 and the related table show the total flow through each branch given as a percentage of the ascending aortic flow.

Invasive pressure wire measurements were acquired in a catheterization laboratory-equipped XMR suite [3]. Pressure was obtained in the ascending aorta (proximal to the coarctation). The proximal systolic, diastolic, and mean pressures were 83.92, 49.68, and 63.35 mmHg, respectively. These values were used to set the parameters for the lumped model. These lumped models are usually composed of a set of resistances and compliances to model the microvascular beds. The compliance influences the transient flow waveform, while the mean value is affected by the resistance only. Due to the assumption that only the mean flow over the cardiac cycle in the BA, LCC, LS and DiaphAo arteries is known, the boundary condition estimation is limited to correctly determining the resistance values at each of these outlets. For estimating the terminal resistance parameter, we use Ohm's law taking into account the flow distribution at the rest state(see the Table in Fig. 2);

$$Q_i * R_i = P_i - P_{out} \qquad (6)$$

where Q_i is the flow at the BA, LCC, LS and DiaphAo arteries, P_i is the mean systolic pressure at the aortic root, P_{out} is the venous pressure for the cardiovascular system and R_i is the flow resistance for each branch-domain. Since the circulation system is not closed, a constant venous pressure

of 5 mmHg is prescribed at the output of each artery [24]. Solving the set of differential-algebraic equations we obtain the following flow resistance for each branch as: $R_{BA} = 7.48 \cdot 10^{11} \text{Pa} \cdot \text{s/m}^3$, $R_{LCC} = 1.50 \cdot 10^{12} \text{Pa} \cdot \text{s/m}^3$, $R_{LS} = 1.28 \cdot 10^{12} \text{Pa} \cdot \text{s/m}^3$ and $R_{DiaphAo} = 1.94 \cdot 10^{11} \text{Pa} \cdot \text{s/m}^3$. Once the total resistances are estimated at these branches, the next step is to distribute the total resistances to the lumped models for all outlets of the 1D cardiovascular domain. To do that we have used a technique based on scaling laws for estimating the blood resistance. This method assumes that the radii and the lengths can be approximated as $R_1 = \varphi R_0$ and $L_1 = \lambda L_0$, being R_0 and L_0 is the radii and the length of the artery at a further distance and φ and λ are constant scaling factors. Therefore for any artery the radii and the length are $R_n = \varphi R_{n-1}$ and $L_n = \lambda L_{n-1}$, respectively. Under the Poiseuille law and assuming that we have 2^n arteries, then the flow distribution is $Q_0/2^n$, and the resistances in the terminal branches can be estimated as follows:

$$\Delta p_n = Q_n \frac{8_n \mu}{\pi R_n^4} \Rightarrow \Delta p_n = \left\{ \frac{\lambda}{2\varphi^4} \right\}^n Q_0 \frac{8 L_0 \mu}{\pi R_0^4} = \left\{ \frac{\lambda}{2\varphi^4} \right\}^n \Delta p_0$$

$$\Delta p_T = \sum_{n=1}^{N} \Delta p_n = \Delta p_0 \sum_{n=1}^{N} \left\{ \frac{\lambda}{2\varphi^4} \right\}^n \quad (7)$$

where Δp_T is the sum of the pressure gradients after each bifurcation through the network, Δp_n is the starting point from the outlet of the terminal artery and N is the number of bifurcations. Dividing Δp_T by Q_0, the resistance $R_\mu T$ can be estimated as:

$$R_{\mu T} = R_{\mu 0} \sum_{n=1}^{N} \left\{ \frac{\lambda}{2\varphi^4} \right\}^n \quad (8)$$

The flow can be approximated using Murray's law [19] as $Q \simeq kr^3$. Therefore $\lambda = \sqrt{0.6}$. Murray's law determines the vessel radius that requires a minimum of energy the vascular system. A relation between φ and λ can be estimated as [26]:

$$\lambda = \frac{N}{N+1} \frac{1}{2\varphi^2} \quad (9)$$

On the other hand, considering the main 55 arteries of the 1D arterial model [35], the R_{BA}, R_{LCC}, R_{LS} and $R_{DiaphAo}$ parameters and taking in account the vessels that arise from BA, LCC, LS and DiaphAo arteries the resistance values for all the terminal branches at the rest condition are finally estimated (see Table 1).

3.1.3 Reduced-order model

In order to settle Eq. 4, we have to define two planes in the 3D geometrical model. The planes chosen were in the ascending aorta (proximal to the coarctation) and in the descending aorta (distal to the coarctation); see Fig. 2. Once these two planes and the inlet and boundary conditions for rest situations are defined, we solve the coupled 3D-1D model. We use an adaptative time step based on the 1D simulation. For each time step, we calculate and store the mean values of the pressure and blood flow for the two planes. These values are then used to estimate the k_1 and k_2 coefficients in (Eq. 4) using a least squares method. The coefficients values found are $k_1 = 3.08 \cdot 10^{-3}$ and $k_2 = 5 \cdot 10^{-4}$, so that function $f^{3D}(k_1, k_2)$ minimizes the sum of the squared pressure drop from the flow values versus the 3D values. Figure 3 (left) shows the pressure drop obtained with the 3D computational values and the reduced-order model. The mean error between the CFD pressure drop and the 3D reduced-order model is 3 %. Figure 3 (right) shows the dependence between the pressure drop and the flow. The area below the hysteresis loop is the energy dissipated. If it is low we can estimate the pressure drop by function $f^{3D}(k_1, k_2)$. Thus, the reduced-order model is capable to capture the energy losses provoked by the geometry of the 3D model. The total computation time for the training phase in a standard PC with Linux environment, 32 bit, 4 GB RAM and dual core 2.83 GHz CPU was about 10 h.
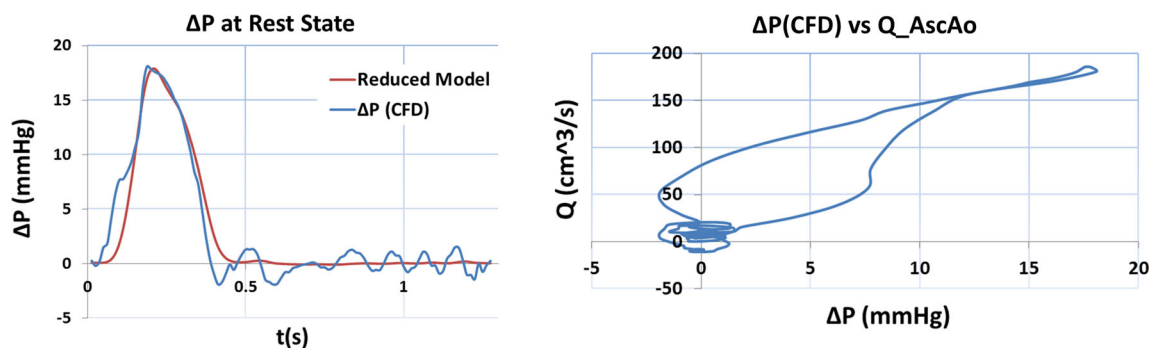
Fig. 3 *Left*: pressure drop between the 3D computational values versus the reduced-order model. *Right*: dependence between the pressure drop and the flow (hysteric loop)

	Total Flow (L/min)	% AscAo
AscAo	13.53	100
BA	3.355	25
LCC	0.6875	5
LS	1.4575	11
DiaphAo	8.03	59
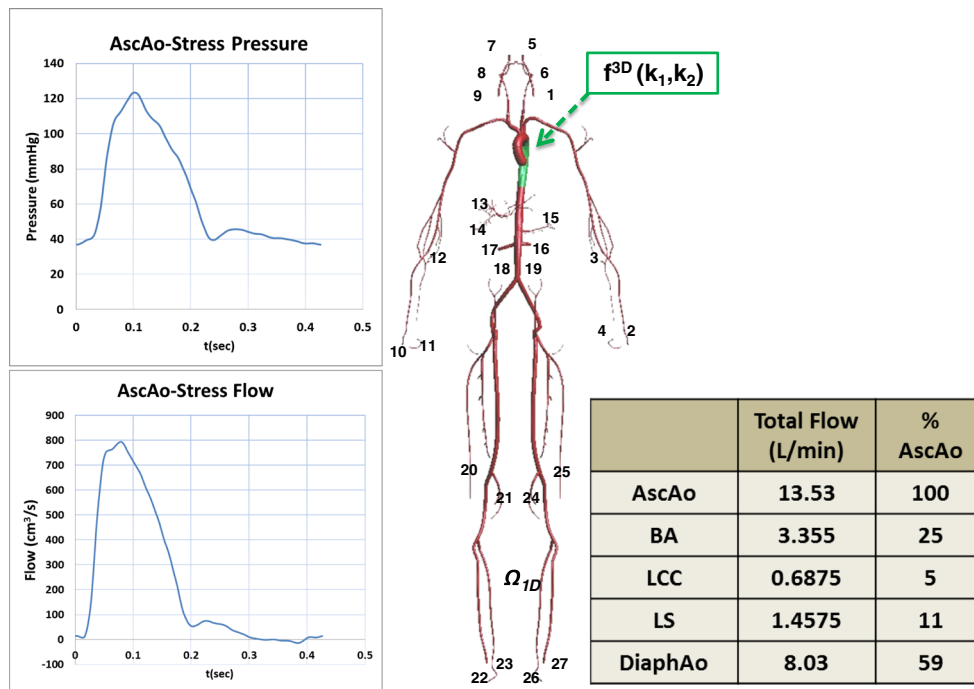
Fig. 4 1D anatomical model based on [35]. Ascending aortic flow waveforms (in cm^3/s) under non-rest conditions as measured by the PC-MRI sequence and ascending aortic pressure (in mmHg) measured with a pressure catheter under non-rest conditions. Table shows the total flow (in L/min) and percentage of ascending aortic flow through the various branches of the aortic model under non-rest conditions. Numbers indicate the terminal branches. Table 1 shows the name and resistance values

3.2 Computation phase

3.2.1 Non-rest situation

Stress (or non-rest) conditions were induced by administering isoprenaline to the patient. Flow and pressure data waveforms were acquired using the same protocol as in rest conditions [3]. The cardiac output of the patient increased to 13.53 L/min and the heart rate to 141 beats per minute (cardiac cycle T = 0.425 s). Figure 4 shows the flow waveform at AscAo. Similar as for a rest situation, the quality of the waveforms at the BA, LCC, and LS arteries was deemed too noisy to be used for the computations. Figure 4 shows the total flow through each branch given as a percentage of the ascending aortic flow. Pressure was obtained in the ascending aorta (proximal to the coarctation). The proximal systolic, diastolic, and mean pressures were 123.35, 36.77, and 64.30 mmHg, respectively (Fig. 4). For estimating the terminal resistance parameters under non-rest situations we have used the same procedure as in rest situations (3.1.2). The results are $R_{BA} = 1.41 \cdot 10^{11}$ Pa $\cdot$ s/m^3, $R_{LCC} = 6.90 \cdot 10^{11}$ Pa $\cdot$ s/m^3, $R_{LS} = 3.25 \cdot 10^{11}$ Pa $\cdot$ s/m^3 and $R_{DiaphAo} = 5.91 \cdot 10^{10}$ Pa $\cdot$ s/m^3. Table 1 shows the terminal resistance values for the terminal vessels for rest and non-rest situations.

Once the terminal resistances for the non-rest condition are set and the parameters k$_1$ and k$_2$ of the 3D reduced-order model are fitted (see Sect. 3.1.3). We are able to estimate the pressure drop under non-rest conditions. For this purpose, we impose the flow profile (Fig. 4) in the ascending aorta of the 1D model. In Fig. 5 the pressure drop under non-rest conditions is shown. The table below shows the mean, systolic and diastolic pressure for the rest and non-rest situations obtained with the reduced-order model. Experimental results are also shown for comparison purposes. The 1D reduced-order model can be also used to simulate other pathological conditions without the necessity to perform the 3D simulation.
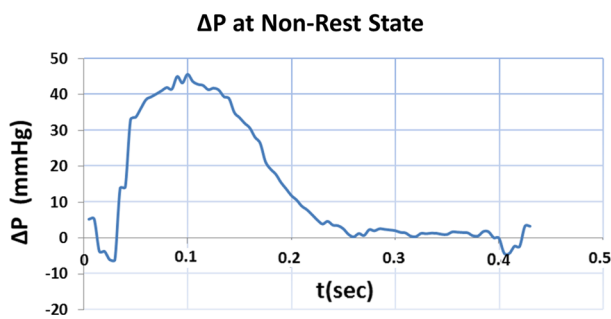
4 Results

From a qualitative point of view, the numerical results shows that the pressure is correctly captured by the reduced-order model (Fig. 3). For the rest situation, the mean (2.83 mmHg) and maximum (18.07 mmHg) pressure drops are estimated using the 3D-1D coupling model. For the non-rest situation, the mean and maximum pressure drops of 13.68 and 44.06 mmHg are estimated using the 1D-reduced-order model. These values are in agreement with previous studies [3,13]. In the rest situation, the reduced model is able to capture the pressure drop with an error under 3 %. Note that the methodology used for parameter estimation can be improved

Table 1 Resistance values for the cardiovascular model in Fig. 4

	Artery name	R_{Rest}	$R_{Non\text{-}rest}$		Artery name	R_{Rest}	$R_{Non\text{-}rest}$
1	Right vertebral	29.6	7.52	15	Intercostals	4.47	1.36
2	Right radius	0.68	0.14	16	Renal	0.68	2.02
3	Right interosseous	4.5	1.14	17	Inferior mesenteric	0.68	2.02
4	Right ulnar	4.5	1.14	18	Superior mesenteric	0.68	2.02
5	Right int. carotid	34.6	15.9	19	Splenic	0.68	2.02
6	Right ext. carotid	34.6	15.9	20	Left ext. iliac	0.10	0.0315
7	Left int. carotid	29.6	7.52	21	Left deep femoral	0.10	0.0315
8	Left ext. carotid	29.6	7.52	22	Left posterior tibial	0.0157	0.00479
9	Left vertebral	17.3	3.27	23	Left anterior tibial	0.0157	0.00479
10	Left radius	0.4	0.075	24	Right ext. iliac	0.10	0.0315
11	Left interosseous	2.63	0.49	25	Right deep femoral	0.0157	0.00479
12	Left ulnar	2.63	0.49	26	Right posterior tibial	0.0157	0.00479
13	Hepatic superior	4.47	1.36	27	Right anterior tibial	0.10	0.0315
14	Gastric	4.47	1.36				

R is the terminal resistance (10^9Pa s/m^3) for the rest and non-rest situations based on the experimental measurements from [35]

	Rest (CFD)	Rest (Exp)	Non-Rest (CFD)	Non-Rest (Exp)
Mean Pressure	60.61	63.35	61	64.30
Max Pressure	97.99	83.917	136.71	123.35
Min Pressure	46.37	49.68	31.59	36.77
Mean ΔP CoA	2.83	-	13.86	-
Max ΔP CoA	18.07	-	45.66	-

Fig. 5 Pressure drop for non-rest situation and CFD results versus experimental results. Pressures are in mmHg. CoA represents the coarctation and ΔP the pressure drop

with the objective of avoiding the oscillatory behavior of the pressure in the descending aorta. Some authors [11,36] use the three-element Windkessel model for improving the fitting of the lumped model. The approach used in this work is however much simpler in the mathematical treatment, while still being able to match the systolic, diastolic and mean pressure values.

5 Conclusion

We have presented a CFD framework which combines patient-specific model and a reduced-order model to estimate the energy losses in cardiovascular problems. The framework has been evaluated with a patient-specific aortic coarctation(CoA) under non-rest and rest situations with satisfactory results. The procedure consists of a two step process. First a reduced-order model is trained using a coupled 1D-3D FEM analysis and then is used together with a 1D solver

under different pathological conditions. The reduced-order model is expressed as a sum of the viscous and turbulent terms, and it is capable to capture the energy losses provoked by the anatomy shape. The error of the reduced-order model is acceptable to capture the pressure drop over two sections of the 3D FEM model. We have modified the 1D formulation in order to integrate the reduced-order model into the framework developed. Results demonstrate that the reduced model is robust with respect to changes in the pathological conditions for patient-specific cases. In order to apply the procedure for a new patient, the framework developed requires a patient-specific model and knowledge of the pathological conditions in a rest situation. In terms of clinical diagnosis the most important feature to be captured is the pressure drop which can be estimated under non-rest situations. The main advantage of the proposed framework is that it relies only on measurements acquired during a rest situation. Then, it can be used under non-rest or rest conditions in a small computation time. The most important numerical approximation intro-

duced in this work is that the training of the reduced-order model is performed using the 3D patient-specific anatomical data considering the boundary conditions taken from the 1D model. The advantage is a great reduction of the computational time versus the fully coupled analysis. The numerical results show that the 1D model retrofitted by using the trained reduced model correctly captures the pressure gradient and the energy losses in cardiovascular diseases.

References

1. Alastruey J, Khir AW, Matthys KS, Segers P, Sherwin SJ, Verdonck PR, Parker KH, Peiró J (2011) Pulse wave propagation in a model human arterial network: assessment of 1-D visco-elastic simulations against in vitro measurements. J Biomech 44(12):2250–2258
2. Bazilevs Y, Takizawa K, Tezduyar TE (2013) Computational fluid-structure interaction: methods and applications. ISBN: 978-0-470-97877-1. p 404
3. CFD Challange: Patient-Specific Hemodynamics at Rest and Stress through an Aortic Coarctation. 2013. http://www.vascularmodel.org/miccai2013/
4. Cristiano A, Malossi I, Blanco PJ, Crosetto P, Deparis S, Quarteroni A (2013) Implicit coupling of one-dimensional and three-dimensional blood flow models with compliant vessels. Multiscale Model Simul 11(2):474–506
5. Dadvand P, Rossi R, Oñate E (2010) An object-oriented environment for developing finite element codes for multi-disciplinary applications. Arch Comput Methods Eng 17:253–297
6. Dadvand P, Rossi R, Gil M, Martorell X, Cotela J, Juanpere E, Idelsohn SR, Oñate E (2013) Migration of a generic multi-physics framework to HPC environments. Comput Fluids 80(10):301–309
7. Formaggia L, Nobile F, Quarteroni A, Veneziani A (1999) Multi-scale modelling of the circulatory system: a preliminary analysis. Comput Vis Sci 2:75–83
8. Formaggia L, Lamponi D, Quarteroni A (2003) One dimensional model for blood flow in arteries. J Eng Math 47:251–276
9. Formaggia L, Gerbeau JF, Nobile F, Quarteroni A (2001) On the coupling of 3D and 1D Navier-Stokes equations for flow problems in compliant vessels. Comput Methods Appl Mech Eng 191:561–582
10. GiD (2011) The personal pre and postprocessor, http://www.gidhome.com CIMNE
11. Ismail M, Wall WA, Gee MG (2013) Adoint-based inverse analysis of windkessel parameters for patient-specific. Vasc Models J Comput Phys 244:113170
12. Itu L, Sharma P, Ralovich K, Mihalef V, Ionasec R, Everett A, Ringel R, Kamen A, Comaniciu D (2013) Non-invasive hemo-dynamic assessment of aortic coarctation: validation with in vivo measurements. Ann Biomed Eng 41:669–681
13. LaDisa JJ et al (2011) Computational simulations for aortic coarctation: representative results from a sampling of patients. J Biomech Eng 133(9):091008–091017
14. LaDisa JJ, Dholakia RJ, Figueroa CA, Vignon-Clementel IE, Chan FP, Samyn MM, Cava JR, Taylor CA, Feinstein JA (2011) Computational simulations demonstrate altered wall shear stress in aortic coarctation patients treated by resection with end-to-end anastomosis. Congenit Heart Dis 6:432–443
15. Lantz J, Ebbers T, Engvall J, Karlsson M (2013) Numerical and experimental assessment of turbulent kinetic energy in an aortic coarctation. J Biomech 46(11):1851–1858
16. Lorensen WE, Cline HE (1987) Marching cubes: a high reso-lution 3d surface construction algorithm. In: Proceedings of SIGGRAPH, pp 163–169
17. Malossi A, Blanco PJ, Crosetto P, Deparis S, Quarteroni A (2013) Implicit coupling of one-dimensional and three-dimensional blood flow models with compliant vessels multiscale modeling. Simulation 11(2):474–506
18. Manguoglu M, Takizawa K, Sameh AH, Tezduyar TE (2010) Solution of linear systems in arterial fluid mechanics computations with boundary layer mesh refinement. Comput Mech 46:83–89
19. Murray CD (1926) The physiological principle of minimum work: I. The vascular system and the cost of blood volume. Proc Natl Acad Sci USA 12(3):207–214
20. Perdikaris P, Karniadakis GE (2014) Fractional-order viscoelasticity in one-dimensional blood flow models. Ann Biomed Eng, pp 0090–6964
21. Quartapelle L (1993) Numerical solution of the incompressible Navier-Stokes equations. Birkhauser Verlag, Basel
22. Raghu R, Vignon-Clementel IE, Figueroa CA, Taylor CA (2011) Comparative study of viscoelastic arterial wall models in nonlinear one-dimensional finite element simulations of blood flow. J Biomech Eng 133:081003–081011
23. Ralovich K et al (2012) Hemodynamic assessment of pre-and post-operative aortic coarctation from MRI. In: Ayache N, Delingette H, Golland P, Mori K (eds) MICCAI 2012, Part II, vol 7511., LNCSSpringer, Heidelberg, pp 486–493
24. Reymond P (2011) Pressure and flow wave propagation in patient-specific models of the arterial tree. PhD Thesis, École Polytechnique Fédérale de Lausanne
25. Reymond P, Merenda F, Perren F, Rafenacht D, Stergiopulos N (2009) Validation of a one-dimensional model of the systemic arterial tree. Am J Physiol Heart Circ Physiol 297(1):H208–H222
26. Sherman TF (1981) On connecting large vessels to small. The meaning of Murray's law. J Gen Physiol 78(4):431–453
27. Sherwin SJ, Franke V, Peiró J, Parker KH (2003) One-dimensional modelling of a vascular network in space-time variables. J Eng Math 47:217–250
28. Steele BN, Valdez-Jasso D, Haider MA, Olufsen MS (2011) Predicting arterial flow and pressure dynamics using a 1D fluid dynamics model with a viscoelastic wall SIAM. J Appl Math 71(4):1123–1143
29. Takizawa K, Christopher J, Tezduyar TE, Sathe S (2010) Space-time finite element computation of arterial fluid-structure interactions with patient-specific data. Int J Numer Methods Biomed Eng 26:101–116
30. Takizawa K, Moorman C, Wright S, Purdue J, McPhail T, Chen PR, Warren J, Tezduyar TE (2011) Patient-specific arterial fluid-structure interaction modeling of cerebral aneurysms. Int J Numer Methods Fluids 65:308–323
31. Takizawa K, Moorman C, Wright S, Christopher J, Tezduyar TE (2011) Wall shear stress calculations in space-time finite element computation of arterial fluid-structure interactions. Comput Mech 46:31–41
32. Tezduyar TE, Takizawa K, Brummer T, Chen PR (2011) Space-time fluid-structure interaction modeling of patient-specific cerebral aneurysms. Int J Numer Methods Biomed Eng 27:665–1710

33. Torii R, Oshima M, Kobayashi T, Takagi K (2009) Fluid structure interaction modeling of blood flow and cerebral aneurysm. Comput Methods Appl Mech Eng 198:3613–3621

34. Vignon-Clementel IE, Figueroa AC, Jansen KE, Taylor CA (2006) Outflow boundary conditions for three-dimensional finite element modeling of blood flow and pressure in arteries. Comput Methods Appl Mech Eng 195(29–32):3776–3796

35. Wang J, Parker KH (2004) Wave propagation in a model of the arterial circulation. J Biomech 37:457–470

36. Xiao N, Humphrey JD, Figueroa CA (2013) Multi-scale computational model of three-dimensional hemodynamics within a deformable full-body arterial network. J Comput Phys 244:22–40